Growth and Decay of Error in a Numerical Cloud Model Due to Small Initial Perturbations and Parameter Changes

QIHANG LI AND RAFAEL L. BRAS

Department of Civil and Environmental Engineering, Massachusetts Institute of Technology, Cambridge, Massachusetts

SHAFIQUL ISLAM

Department of Civil and Environmental Engineering, University of Cincinnati, Cincinnati, Ohio

(Manuscript received 8 April 1994, in final form 31 December 1994)

ABSTRACT

The behavior of a numerical cloud model is investigated in terms of its sensitivity to perturbations with two kinds of lateral boundary conditions: 1) with cyclic lateral boundary conditions, the model is sensitive to many aspects of its structure, including a very small potential temperature perturbation at only one grid point, changes in time step, and small changes in parameters such as the autoconversion rate from cloud water to rainwater and the latent heat of vaporization; 2) with prescribed lateral boundary conditions, growth and decay of perturbations are highly dependent on the flow conditions inside the domain. It is shown that under relatively uniform (unidirectional) advection across the domain, the perturbations will decay. On the other hand, convergence, divergence, or, in general, flow patterns with changing directions support error growth. This study shows that it is the flow structure inside the model domain that is important in determining whether the prescribed lateral boundary conditions will result in decaying or growing perturbations. The numerical model is inherently sensitive to initial perturbations, but errors can decay due to advection of information from lateral boundaries across the domain by uniform flow. This result provides one explanation to the reported results in earlier studies showing both error growth and decay.

1. Introduction

Growth and decay of perturbations in initial conditions of numerical models are important in numerical weather forecasts. Predictability is a measure of the evolution of such perturbations. Traditionally, two methods have been used in predictability studies. One is the dynamical–empirical method, which is based on turbulence theory; the other is a dynamical method in which two numerical simulations, called the control run and the perturbed run, respectively, are started from slightly different initial conditions. The evolution patterns of model variables in the two runs are then compared and the divergence of solutions from one another is evaluated. The following expression defines the root-mean-square difference between the control and perturbed runs:

$$\mathrm{rms2}(t) = \left\{\frac{1}{N}\sum_{i=1}^{N}[X_{pi}(t) - X_{ci}(t)]^2\right\}^{1/2}, \quad (1)$$

where $X_{ci}(t)$ and $X_{pi}(t)$ denote the values of variable X at grid point i and time t for the respective control and perturbed runs; N is the total number of grid points used in the calculation of $\mathrm{rms2}(t)$.

The measure $\mathrm{rms2}(t)$ can reveal the divergence of two solutions started from slightly different initial conditions. Early estimates of predictability with numerical global models using this measure (e.g., Charney et al. 1966; Kasahara 1972) indicated a limited predictability and show continuous growth of initial perturbations until saturation. More recently, attention has also been directed to mesoscale predictability. Early studies using limited-area models (e.g., Anthes et al. 1985) revealed no significant growth for $\mathrm{rms2}(t)$. Subsequent studies (e.g., Errico and Baumhefner 1987; Paegle and Vukicevic 1987; Vukicevic and Paegle 1989; Berri and Paegle 1990; Vukicevic and Errico 1990), however, showed both growth and decay on various occasions. Some explanations have been given to account for such peculiar behavior of limited-area models. Among other things, the prescription of lateral boundary conditions is believed to be the most important cause for this behavior.

Anthes et al. (1985) found no significant error growth during a 72-h forecast period with their meso-α-scale limited-area model. With a global model, however, they found exponential error growth over the

Corresponding author address: Dr. Qihang Li, Civil and Environmental Engineering, Massachusetts Institute of Technology, Rm 48-208, Cambridge, MA 02139.
E-mail: hang@athena.mit.edu

same mesoscale region. They speculated that the lack of error growth in the limited-area model is caused by the imposition of identical lateral boundary conditions on both the control and the perturbed runs. But further verification of this speculation was not given.

Errico and Baumhefner (1987) tried to analyze and explain the Anthes et al. (1985) results by adopting a new experiment design using new algorithms that did not exist in Anthes et al. (1985), such as the specification of initial perturbations in terms of two-dimensional spectra. Through a series of experiments with perturbations of different wavelength characteristics, they concluded that factors that may be responsible for the limited growth include lateral boundaries, the spatial scale modeled, the numerical methods used (horizontal diffusion), and the length of forecast. They speculated that fixed lateral boundary conditions may result in flows that advect perturbations out of the domain. However, they mentioned that this advective process is slower than the other two processes, namely, gravity wave propagation and horizontal diffusion.

Vukicevic and Paegle (1989) investigated the lateral boundary effect using a barotropic model that can be applied to a global domain as well as to local domains with one-way interacting boundary conditions. They found that the error evolution is dependent on the domain size and to a lesser extent on the domain location. The main conclusion is that if the domain is small enough (about the size of a typical mesoscale model domain), the forecast is insensitive to small initial uncertainties.

In their study of the predictability of a sea-breeze-type circulation over South America, Berri and Paegle (1990) observed error decay for a relatively large domain ($45° \times 45°$, $\Delta x \sim 200$ km) and error growth for smaller domains (320 km $\times$ 420 km, $\Delta x \sim 20$ km). They speculated that the error growth in smaller domains might be a consequence of fast small-scale instabilities that are not resolved and therefore do not contribute to error growth, in the larger-scale experiments.

Vukicevic and Errico (1990) extended the analyses of Vukicevic and Paegle (1989) to a complex baroclinic limited-area model and concluded that the one-way interacting boundaries constrained the evolution of initial perturbations in the same way as observed in the barotropic case of Vukicevic and Paegle (1989). Namely, the initial perturbations grow only in domains larger than a critical size (approximately a 4500-km square for the mesoscale model they were using) and damp in smaller domains. Based on spectral analysis of the error field in the largest domain (8880 km $\times$ 6400 km), they concluded that the one-way interacting lateral boundary conditions constrain the evolution of perturbations by imposing an upper limit upon the horizontal scales that are free to evolve in accordance with the model dynamics. Another conclusion is that the small-scale perturbations contribute to synoptic-scale error growth through an initial upscale transfer of perturbation energy. Therefore, initial error at wavelengths shorter than 1000 km appears to influence synoptic-scale flow evolution, although these shorter scales are not themselves sensitive to initial error. However, they recognized that the latter conclusion was limited to their specific model only and referred to the results of Berri and Paegle (1990), which showed error growth for scales much smaller than 1000 km. Thus, they commented that mesoscale predictability results were case- and model-dependent.

Zeng and Pielke (1993) studied the error-growth dynamics of thermally induced surface circulations using a limited-area model with fine resolution ($\Delta x = 2$ km and 100 m were used in separate experiments). They studied, among other things, the model sensitivity to initial conditions, model parameters, and boundary specifications. One of their findings is that the error growth (at least at the stage when the surface forcing is strong) is not sensitive to the characteristics of the initial perturbations.

Another measure that quantifies the natural variability of a model variable is the root-mean-square difference between the field of the variable at time t and its initial field; namely,

$$\mathrm{rms1}(t) = \left\{ \frac{1}{N} \sum_{i=1}^{N} [X_{ci}(t) - X_{ci}(0)]^2 \right\}^{1/2}. \quad (2)$$

The rms1(t) is also referred to as the signal, and rms2(t) is correspondingly called the noise. It is a common practice among researchers to determine the predictability of a system based on the signal-to-noise ratio. Namely, the system is defined as predictable if the ratio rms1(t)/rms2(t) is larger than unity, and unpredictable if the ratio is smaller than unity.

The definition of predictability based on the signal-to-noise ratio has been used in some studies (e.g., Berri and Paegle 1990; Zeng and Pielke 1993). However, one thing worth noting is that, with such a definition of predictability, a system tends to be more predictable in a transient state than in an equilibrium state. In a transient state, the values of model variables increase or decrease continuously for a relatively long duration, reaching much larger or smaller values relative to the beginning than if the system is in an equilibrium state. Remembering that the signal rms1(t) is the root-mean-square difference between the variable field at time t and the initial field, one can see that the signal tends to reach a larger amplitude in a transient state than in an equilibrium state (since in the equilibrium state, the initial field is also located inside the equilibrium regime). As the noise rms2(t) is the difference between the control run and the perturbed run, if both the control and the perturbed runs can follow the transient trend to some extent, the noise will usually be smaller than the signal, leading to better predictability. Indeed, in a strong transient regime, a small difference in the

initial condition can do little in changing or reversing the trend. For example, a small change in the surface temperature will not severely affect a developing thunderstorm. Such an event, with a strong trend, is relatively more predictable due to its larger signal. In an equilibrium state, however, model variables evolve, or fluctuate, around their equilibrium levels. The signal rms1 (t) in this case is smaller. The model evolution is strongly dictated by the model's nonlinear dynamics. If the model is inherently sensitive to initial perturbations due to nonlinearity, the noise rms2(t) can increase very quickly and reach or exceed the signal in a much shorter time. Thus, it can be said that in a transient state, the role of nonlinearities in the predictability context is masked. If one is interested in the role of nonlinearities, then, it is best to perform the numerical experiments in equilibrium states.

Islam et al. (1993) investigated the predictability of space–time averages of mesoscale precipitation using a numerical cloud model. Numerical experiments in their study were performed in a convective–radiative equilibrium state that was achieved by requiring a balance between the surface heat fluxes and radiative cooling. In this equilibrium state the effect of transients is eliminated, and the predictability in this context is mainly a result of nonlinearities. The model domain was 60 km × 60 km in the horizontal and 20 km deep, with resolutions of 2 km and 250 m in the respective horizontal and vertical directions. Cyclic lateral boundary conditions were used, a major departure from other studies. In their study, only one perturbation experiment was performed in which a random perturbation uniformly distributed between −0.25 and +0.25 K was added to the potential temperature at every grid point. Surface rainfall rates averaged over various space scales and timescales are compared for the control versus perturbed runs to see the quantitative dependence of predictability on these scales. It was shown that the prediction error tended to grow and reach a saturation level, but the time required to do so depended on the space–time averaging scale. As expected, larger averaging scales led to longer predictability time. Since only one perturbation experiment was performed, however, it remains to clarify how the error evolution depends on the characteristics of the perturbation. For example, the perturbation amplitude and location are of particular interest.

This study uses the same numerical cloud model of Islam et al. (1993) to study two additional issues:

- the effect of perturbation characteristics and model parameters on the model evolution;
- the effect of prescribed lateral boundary conditions on predictability; specifically, we address the question of why limited-area models with prescribed lateral boundary conditions show both error growth and decay on various occasions.

As in Islam et al. (1993), we perform our experiments in a convective–radiative equilibrium state in order to focus on the effect of nonlinearities. In addressing the first issue we use cyclic lateral boundary conditions to eliminate the boundary effect for the moment and concentrate on the model dynamics. Cyclic boundary conditions are common in cloud models and have been used in many earlier studies (e.g., Clark and Hall 1979; Tao and Simpson 1989; Zeng and Pielke 1993). Since the predictability measures are only an average of prediction errors at many grid points in the domain, it is important, when evaluating the growth or decay of a measure, to examine the spatial shape and temporal evolution of the error field. This approach is particularly effective in addressing the second issue.

In the rest of this paper, sections 2 and 3 address the first and the second issues, respectively, and our conclusions are provided in section 4.

2. Perturbation experiments with cyclic lateral boundary conditions

This section discusses the sensitivity of the model to perturbation characteristics and other model aspects. Specifically, we want to see whether and how the error will grow if the initial perturbation is very small and localized, and how the model responds to small changes in model parameters. Since cyclic lateral boundary conditions are used, attention will also be paid to see whether the error will grow until saturation as seen in early studies with global models. A brief description of the model is presented first, followed by perturbation experiments.

a. The model and the quasi-equilibrium state

A numerical cloud model developed by Clark (1977, 1979) and his collaborators (e.g., Clark and Hall 1979; Clark and Farley 1984) at NCAR was used in our study. The model is a finite-difference approximation to the anelastic, nonhydrostatic fluid dynamics equations with expansion of the system variables around profiles of an idealized atmosphere with constant stability (linear potential temperature profile). The finite-difference formulation employs the Arakawa (1966) and Lilly (1965) second-order algorithm for the conservation of momentum combined with the second-order-accurate, positive-definite advection transport algorithm of Smolarkiewicz (1984) for conservation equation of all thermodynamical variables. The subgrid-scale turbulent processes are parameterized using the first-order closure of Lilly (1962) and Smagorinsky (1963). The phase change of water substance is evaluated with the assumption that 100% humidity is maintained within the cloud, and precipitation development is restricted to warm rain through the Kessler (1969) parameterization.

To focus on the effect of the model equation's nonlinearities and to carry out valid statistical analyses of

the evolution of model variables, we need these variables to be in an equilibrium state. In our study, this is achieved by maintaining a constant forcing (sensible and latent heat flux from the surface) and running the model sufficiently long. The model then enters a statistical equilibrium state where the model variables fluctuate around their mean values corresponding to the forcing. We call this a quasi-equilibrium state.

All simulations were performed in a two-dimensional framework. Topography is not considered here. We choose a model domain of 240 km horizontally and 20 km vertically, using the uppermost 5-km layer as a Rayleigh friction absorber to reduce the reflection of vertically propagating gravity waves. As shown by Islam (1991) and in our present simulation, this domain size is large enough for a characteristic mesoscale cloud system to develop. A grid size of 1 km (horizontal) × 0.25 km (vertical) is employed. A sounding (Jordan 1958) typical of the tropical atmosphere—including pressure, wind, temperature, and water vapor profiles—was used as the initial environment. For simplicity, however, zero wind was assumed in some of our experiments and a uniform wind of 10 m s^{-1} was used for the rest. A radiative–convective equilibrium model atmosphere is simulated by providing a constant sensible heat flux $Q_s = 166$ W m^{-2} and latent heat flux $Q_l = 332$ W m^{-2} from the surface. This corresponds to a total heat flux of $Q = Q_s + Q_l = 498$ W m^{-2} and an evaporation rate of 11.5 mm day^{-1} or 0.48 mm h^{-1} into the model domain. To balance this heat and moisture flux, a constant cooling rate of 6°C day^{-1} is applied to the potential temperature field below tropopause. We expect that, in the quasi-equilibrium state, the surface rainfall rate will balance the evaporation rate. The model is started from rest, and the initial motion is created by adding a noise to the linearly increasing surface sensible heat flux during the initial 30 min; that is, the sensible heat flux at a grid point has the form $Q_s(t) = (t/1800)166\epsilon$ W m^{-2} for $t \leqslant 1800$ s, where ϵ is a random variable uniformly distributed between 0.9 and 1.1. For time greater than 1800 s the sensible heat flux Q_s is 166 W m^2 everywhere. The time step is set to 10 s and cyclic lateral boundary conditions are used in this first set of experiments.

Under these initial and boundary conditions, the model was run for 60 h. A look at the evolution of various model variables, particularly the domain-averaged surface rainfall rate, reveals that they vary violently at the beginning, but, after about 40 h, gradually subside to a relatively stable state where the variables fluctuate around what seem to be their mean values. In the case of domain-averaged surface rainfall rate (see Fig. 1), for example, the fluctuation is large before 40 h, ranging from 0 to 8 mm h^{-1} (based on 5-min accumulated amount), but it becomes relatively stable afterward and fluctuates around the constant surface evaporation rate of 0.48 mm h^{-1}. The typical surface rainfall pattern can be seen in Fig. 3b, where

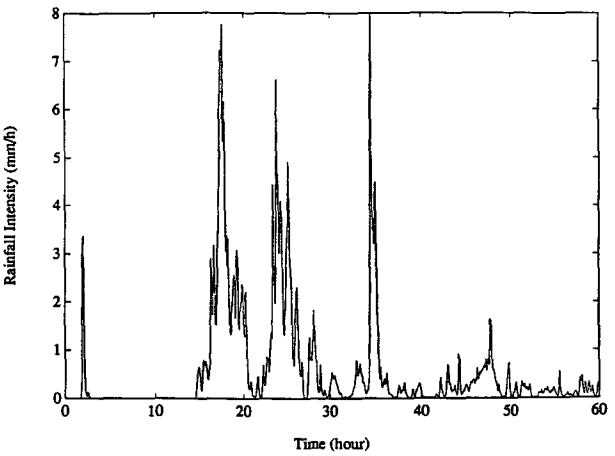

FIG. 1. Domain-averaged surface rainfall series (based on 5-min accumulated amount).

the x–t diagram of surface rain rate is shown. The time span is from 60 to 65 h (notice that, in all figures except Fig. 1, the time indicated is relative to 60 h). The only contour level used here is 1 mm h^{-1}, which is intended to delineate the rain cell boundaries. It can be observed that at any instant there are several rain cells distributed over the 240-km domain. A typical rain cell, as defined by the 1 mm h^{-1} contour, is a few kilometers wide and lasts about half an hour. However, a relatively long-lasting cell appears along the cyclic boundary. It is not clear whether or not this happens by chance. Such phenomenon was not observed by Islam (1991), where the same model was used.

b. Perturbation experiment design and results

We want to see how the model responds to small perturbations in its initial conditions and model parameters under cyclic lateral boundary conditions. We will show how the model evolution is affected by small changes in the initial value of a particular variable, in a parameter, or in time step. The objective of perturbing model parameters is to verify the speculation that if the model is sensitive to initial conditions, it must be sensitive to changes in model parameters too. Each experiment is composed of two simulations that start from slightly different initial conditions or possess slightly different values for a particular parameter. All simulations were run for 20 h (from 60 to 80 h). The state at 60 h is taken as initial condition for the control run, and perturbations in model parameters or initial conditions are introduced for perturbed runs. Specifically, the following six experiments were performed.

Experiment 1. A perturbation [−0.025°C, +0.025°C] is introduced into every grid point of the initial potential temperature field; here [−0.025°C, +0.025°C] denotes a random perturbation uniformly distributed in the interval from −0.025°C to +0.025°C.

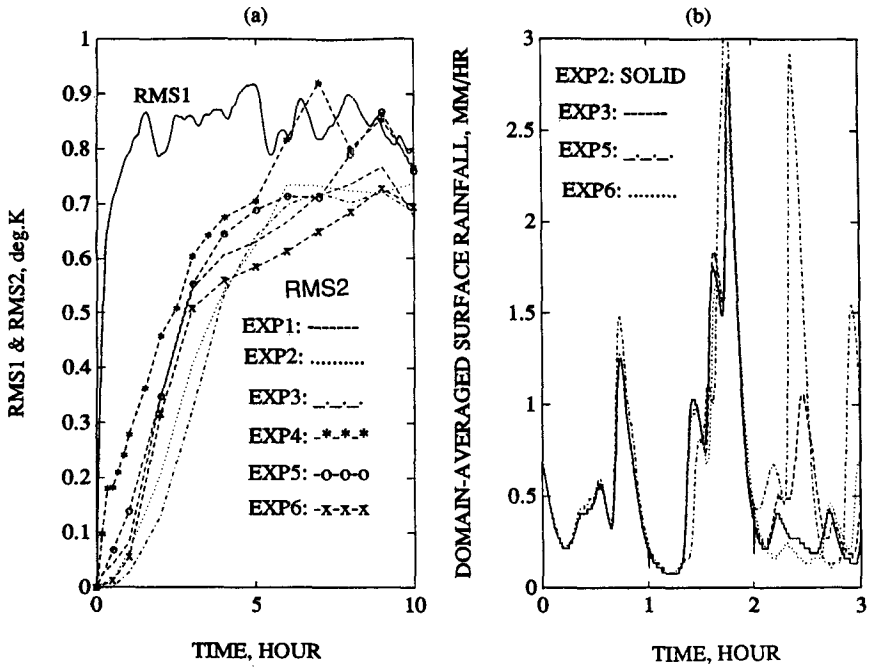

FIG. 2. (a) Error evolution of potential temperature field for the six experiments with cyclic lateral boundary conditions. (b) Domain-averaged surface rainfall.

Experiment 2. A perturbation of [−0.025°C, +0.025°C] is applied to grid points at the 5-km level only.

Experiment 3. A fixed perturbation of +0.025°C is applied to one grid point only, which is located at the 5-km level and in the middle of the domain.

Experiment 4. The control run and the perturbed run are exactly the same except that the integration time step is 10 s for the control run and 5 s for the perturbed run.

Experiment 5. The control run and the perturbed run are exactly the same except that the latent heat of vaporization is 2.5×10^6 J kg^{-1} for the control run and 2.525×10^6 J kg^{-1} for the perturbed run, a 1% difference.

Experiment 6. The same as experiment 5 except that the parameter changed is the autoconversion rate, AO1, which represents the rate at which cloud water is converted into rainwater. We set AO1 = 0.001 s^{-1} for the control run and AO1 = 0.00101 s^{-1} for the perturbed run, also a 1% difference.

Since all the perturbed runs share a common control run, we apply the measure rms1 (the signal) to that common control run only. The measure rms2 (the noise) is applied to every perturbed run and is compared with rms1. In computing rms1 and rms2, those grid points above the tropopause (13 km) are excluded because most of them are inside the gravity wave filter. The model variables whose evolutions are studied include horizontal and vertical velocities, potential temperature, vapor mixing ratio, cloud water mixing ratio, rainwater mixing ratio and domain-averaged surface rainfall rate. Comparisons between rms1 and rms2 for each of these variables show that error growth occurs in all of them. To save space, plots are shown only for the potential temperature and domain-averaged surface rainfall rate and for the initial 10 and 3 h, respectively (see Fig. 2). Fig. 2a contains one rms1 curve for the control run and six rms2 curves for the six perturbed runs, and Fig. 2b contains domain-averaged surface rainfall series for experiments 2, 3, 5, and 6. In Fig. 2b we do not use rms1 and rms2 to evaluate the divergence. Because there is only one value for the domain-averaged rainfall rate at any instant, it is more straightforward to directly compare the rainfall series.

The rms1 measure (the signal) for every variable reaches a saturation value sooner or later, led by vertical velocity (not shown), which takes only 15 min to reach its saturation value of about 0.5–0.6 m s^{-1}. Some other variables, such as potential temperature shown in Fig. 2a, take 1–2 h to attain saturation. In Fig. 2b, domain-averaged surface rainfall for different experiments diverges after 2 h. The rms2 (the noise) grows at roughly the same rate for all perturbation runs, and approaches the rms1 curve in a few hours. It is important to note that, even though the initial perturbation in experiment 3 can be considered very small (only 0.025°C at one point), it nevertheless grows at a rate not materially slower than in experiments 1 and 2, although it does have a smaller magnitude during the first few hours.

This shows that the system is very sensitive to initial perturbations, and the error will grow to saturation regardless of the characteristics and location of perturbation (for the cyclic lateral boundary conditions). It is also interesting to note that rms2 for experiments 4–6, with perturbed model parameters, grows faster and larger than those for the initial condition experiments (experiments 1–3). These features, we speculate, imply that changing the values of model parameters makes the system slightly different dynamically with also a slightly different equilibrium level.

The divergence between the control and perturbed runs in experiment 4, in which time steps of 10 and 5 s were used, is interesting. A valid question is whether this divergence might have been caused by unsuspected instabilities due to the use of a 10-s time step rather than a smaller one. To clarify this issue, a separate experiment was performed with time steps halved—that is, 5 s for the control run and 2.5 s for the perturbed run. Surface rainfall rate produced from the two runs are compared in Figs. 3a–d. Figure 3a shows domain-averaged surface rain rates for the control run (first 10 h, i.e., from 60 to 70 h, solid curve) and the perturbed run (first 5 h, i.e., from 60 to 65 h, dashed curve). These rain rates begin to diverge after about 2 h. Figures 3b and 3c are Hovmöller diagrams (x–t section) of the surface rain rate, where the only contour level is 1 mm h^{-1} (to delineate the boundary of the rain cells). Figure 3d represents the absolute differences between Fig. 3b and 3c. Thus, Figs. 3b–d show the spatial and temporal differences in surface rainfall between the two runs. During the first 1–2 h the two rainfall fields are similar spatially and temporally (see Figs. 3b and 3c) and the differences are small (see Fig. 3d), but greater differences begin to emerge afterward. This result indicates that the divergence is not caused by instabilities, but is indeed the result of the model's nonlinearities.

Experiments in this section serve to demonstrate the extreme sensitivity of the model to changes in initial conditions or parameters. With regard to predictability, it can be said that a limited-area model with cyclic lateral boundary conditions is not fundamentally different from a global model in terms of its error dynamics.

3. Perturbation experiments with prescribed lateral boundary conditions

This section focuses on the question of why error in limited-area models with prescribed lateral boundary conditions grows on one occasion and decays on another. By analyzing results from many experiments with prescribed lateral boundary conditions, we have come to the realization that the flow pattern inside the model domain is the controlling factor through which the lateral boundaries exert their limiting effect. To

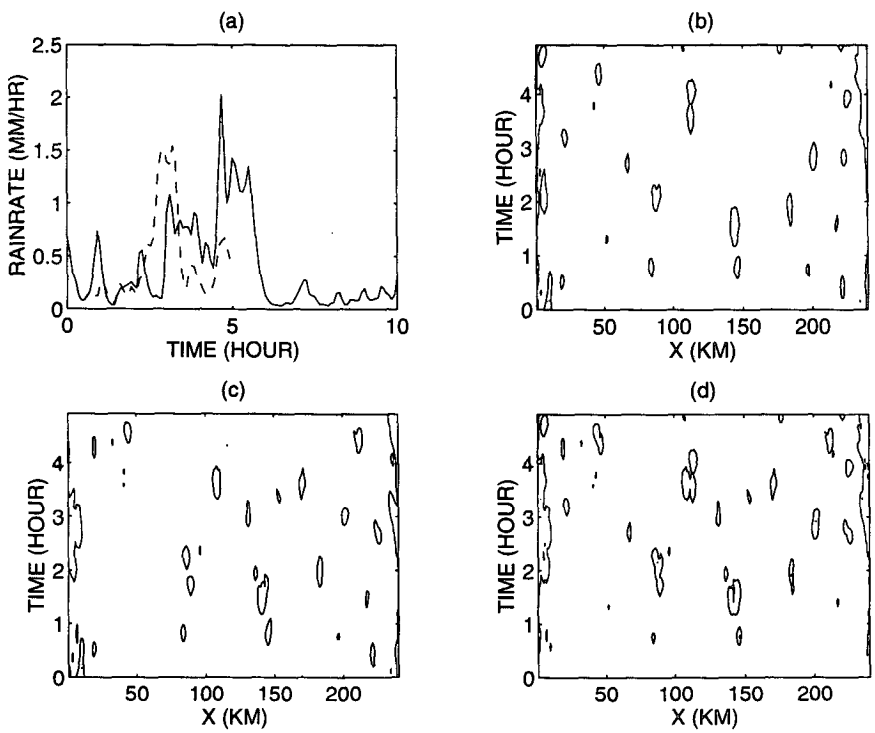

FIG. 3. (a) Domain-averaged surface rain rate; solid: control run, 5-s time step; dashed: perturbed run, 2.5-s time step. (b) and (c) The x–t sections of surface rainfall field for control and perturbed runs; the only contour level shown is 1 mm h^{-1}. (d) Absolute differences between (b) and (c).

show this we discuss three experiments with different flow patterns.

a. Flow pattern without prevailing wind direction

In this experiment the cloud model was run with two nested domains, with the outer domain providing lateral boundary conditions to the inner one. The outer domain itself still maintains cyclic lateral boundaries. This is a one-way interacting mode—that is, the outer domain is not influenced by the inner domain. The outer domain size is 240 km × 20 km, as in the cyclic boundary condition case, with a resolution of 4 km (horizontal) by 1 km (vertical). The inner domain is 120 km × 15 km with a resolution of 1 km by 0.25 km, and is located in the middle of the outer domain. As in the cyclic boundary condition case, the model uses the data at 60 h as its initial condition. It should be remembered here that in establishing our equilibrium state we have started the model from rest, so that the resulting flow field inside the model domain has no prevailing directions due to uniform energy fluxes from the surface.

In the variation experiment, a uniformly distributed perturbation of [−0.25 K, +0.25 K] was added to the potential temperature field at every grid point of the inner domain. Results are shown in Fig. 4. Figure 4a shows continuous error growth, indicating that in this case the imposed boundary conditions fail to constrain error growth due to the absence of prevailing wind direction within the domain as shown in Fig. 4b, where the heavily contoured areas indicate left-to-right flows and the white areas represent right-to-left flows. The prescribed lateral boundary conditions fail to constrain error growth because errors cannot be effectively advected out of the domain. Figures 4c and 4d show potential temperature error fields at 5 and 15 h, respectively. It can be seen that errors spread over the whole domain.

To confirm the effects of prevailing wind direction on error growth, we performed further experiments as described in sections 3b and 3c.

b. Flow pattern with a prevailing wind direction and a portion of return flow

To create a wind field with a prevailing direction, we set the initial horizontal velocity to 10 m s^{-1} from left to right everywhere and reran the model for 60 h to reach equilibrium. A perturbation experiment was performed whereby a very small initial error of +0.025 K was introduced at only one point located at the middle

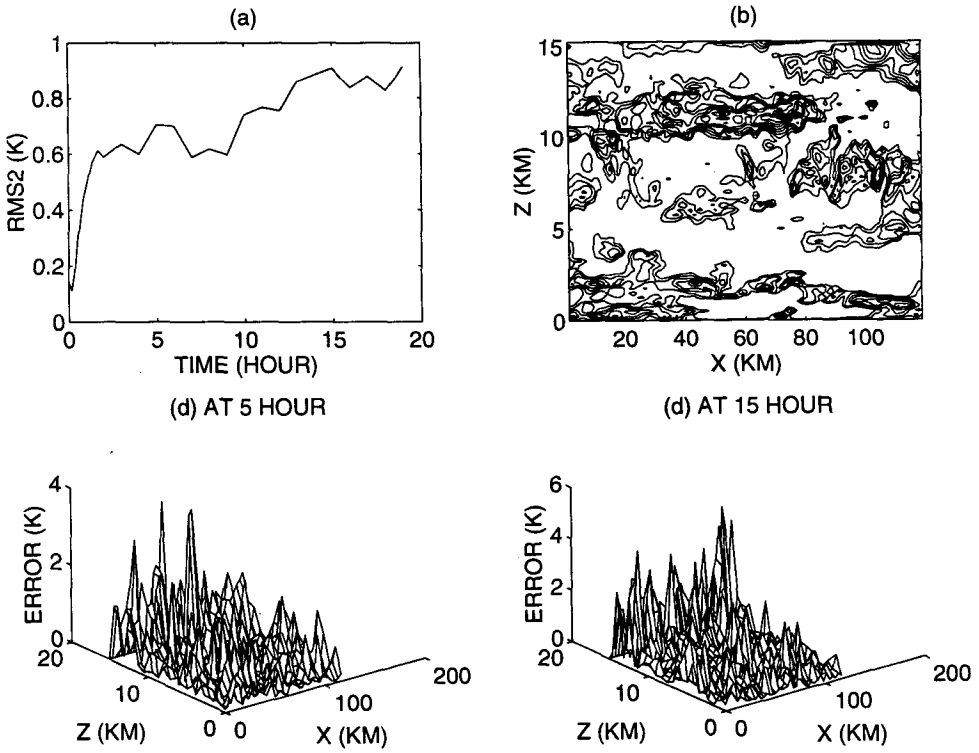

FIG. 4. (a) Error evolution of potential temperature field: prescribed lateral boundary conditions plus flow without prevailing directions. (b) Horizontal velocity pattern at 15 h. Heavily contoured areas show left-to-right flow (ranging from 0 to 10 m s^{-1}), white areas are right-to-left flow. (c) and (d) Potential temperature error fields at 5 and 15 h.

of the inner domain and 5 km from the ground. The simulation was run from 60 to 80 h. The rms2 for the potential temperature field in the inner domain is shown in Fig. 5a (only for the initial 10 h) where curve 1 is for the whole inner domain and curve 2 is for a portion indicated by a rectangle in Fig. 5b. Curve 2 in Fig. 5a is intended to show that error growth rate may be different for different regions of the domain. Curve 2 grows more slowly and to a smaller amplitude than curve 1, because the region represented by curve 2 is located immediately downstream from the left boundary and the flow in it is almost unidirectional, enabling the prescribed boundary conditions to be advected across and eliminate the initial perturbations. However, curve 2 does not decay to zero because a unidirectional flow has not been maintained for that region throughout the experiment. The fact that curve 1, which represents the whole inner domain, does not decay indicates that the prescribed boundary conditions also fail to constrain the error growth in this case. This is due to the presence of return flows in the domain, as indicated by dashed contours in the horizontal velocity pattern of Fig. 5b. Comparing curves 1 and 2 illustrates how the lateral boundary exerts its limiting effect through the flow pattern. It is helpful to visualize the above argument by looking at Fig. 5c and 5d, where the error fields (absolute differences between the potential temperature fields of the control and perturbed runs) at 5 and 9 h are plotted. Since we introduced a small error of 0.025 K at only one point at the beginning, Fig. 5c and 5d show how quickly errors spread all over the domain. However, the distribution of errors over the domain is not uniform, as evident from a strip of relatively smaller error in the upper-middle part of the domain (see arrows). Such a distribution is closely related to the flow field. The horizontal velocity field at 9 h is shown in Fig. 5b, in which solid contours represent left-to-right motions and dashed contours indicate right-to-left motions (which we call return flows). It can be observed that the main flow is from left to right, but there are some return flows at the top and the lower-middle part of the domain. The strip of smaller error is collocated with the main flow, which obviously has been able to advect the boundary conditions across its path, making the errors there small. However, although errors can be reduced along the path, they cannot be completely removed, because they are carried back to the left by the return flows adjacent to the main flow, and then join the main flow again.

To further demonstrate the effects of flow pattern, we have performed another experiment in which the entire inner domain is located inside the above-men-

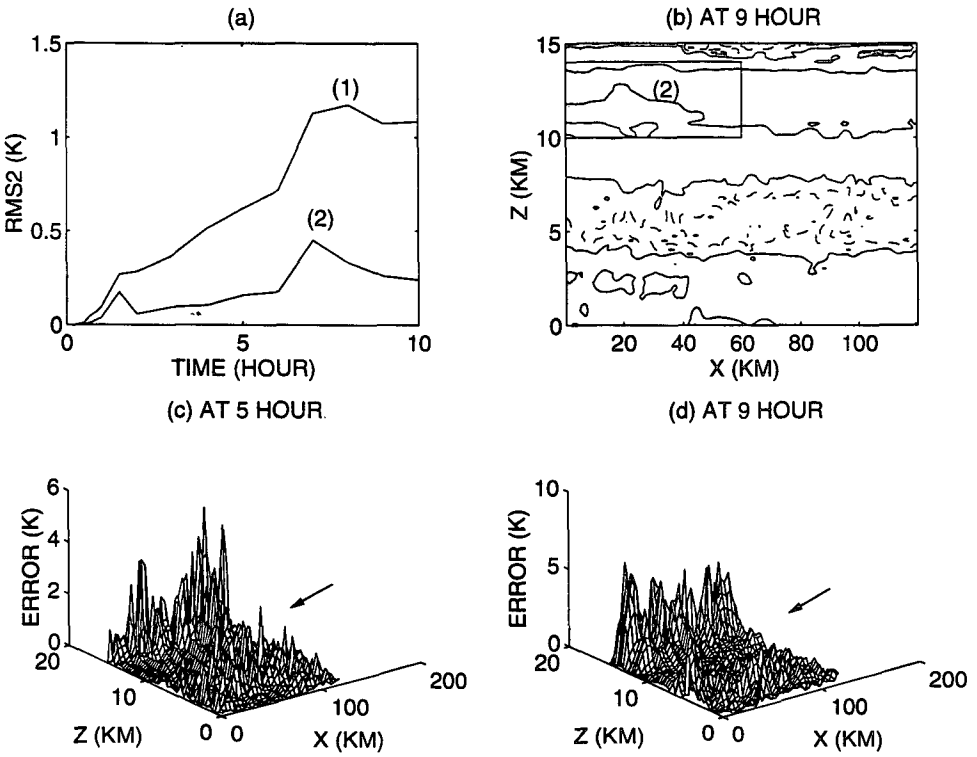

FIG. 5. (a) Error evolution of potential temperature field: prescribed lateral boundary conditions plus flow with a prevailing direction and some return flows. Curve 1: whole domain; curve 2: partial domain. (b) Horizontal velocity pattern at 9 h showing areas of different flow directions. Dashed contours indicate return flows. (c) and (d) Error fields of potential temperature at 5 and 9 h.

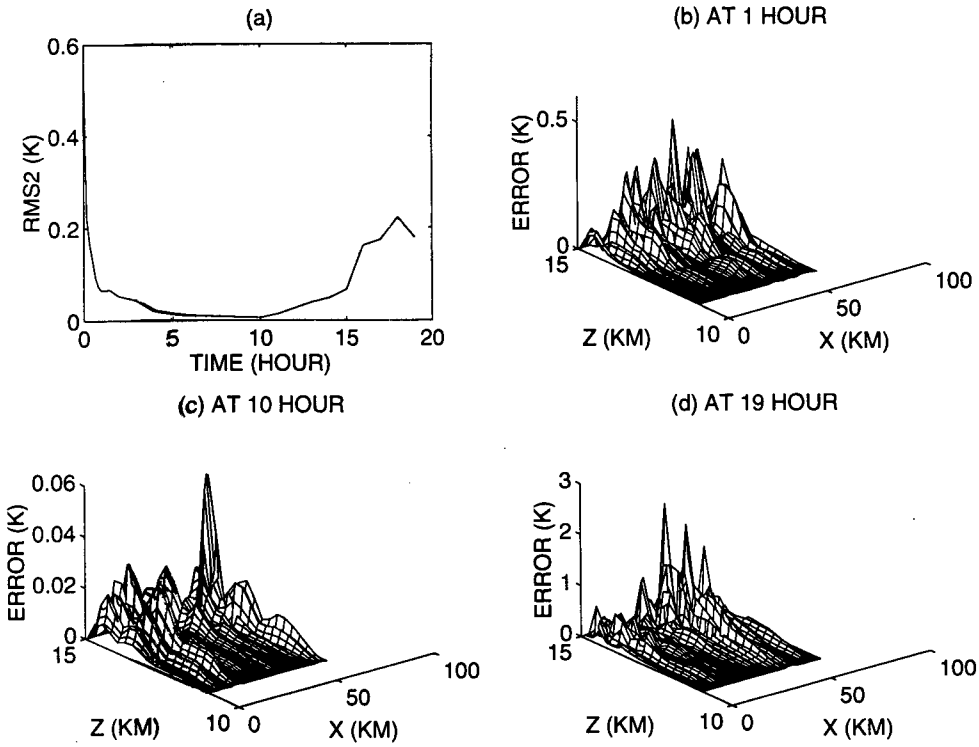

FIG. 6. (a) Error evolution of potential temperature field: prescribed lateral boundary conditions plus flow with a prevailing direction and a very small portion of return flow. (b)–(d) Error fields of potential temperature at 1, 10, and 19 h, respectively.

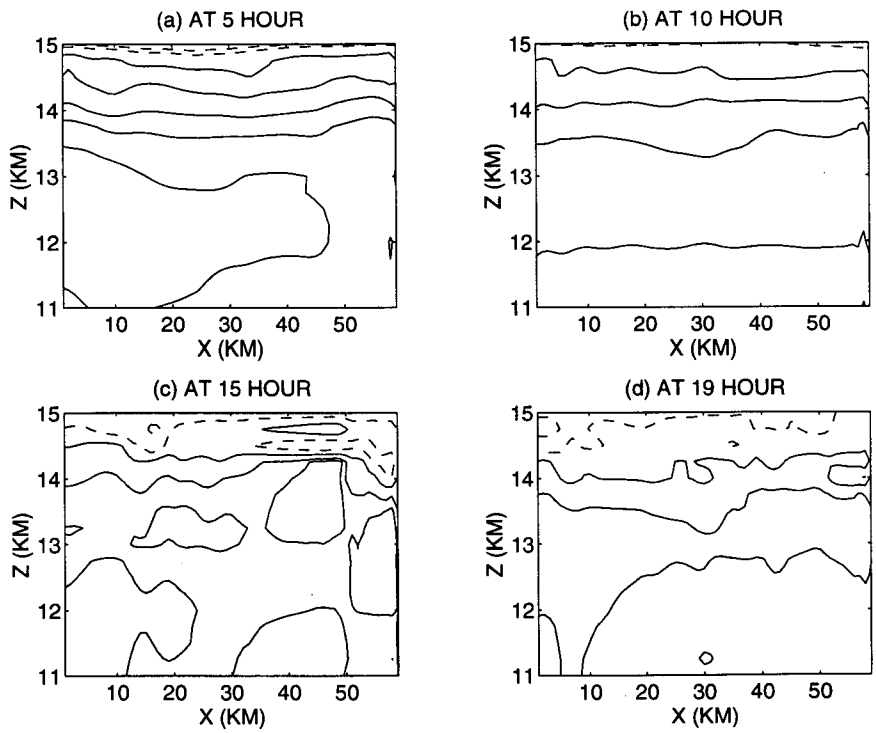

FIG. 7. (a)–(d) Horizontal velocity patterns at 5, 10, 15, and 19 h, respectively, showing areas of different flow directions. For the same case as Fig. 6.

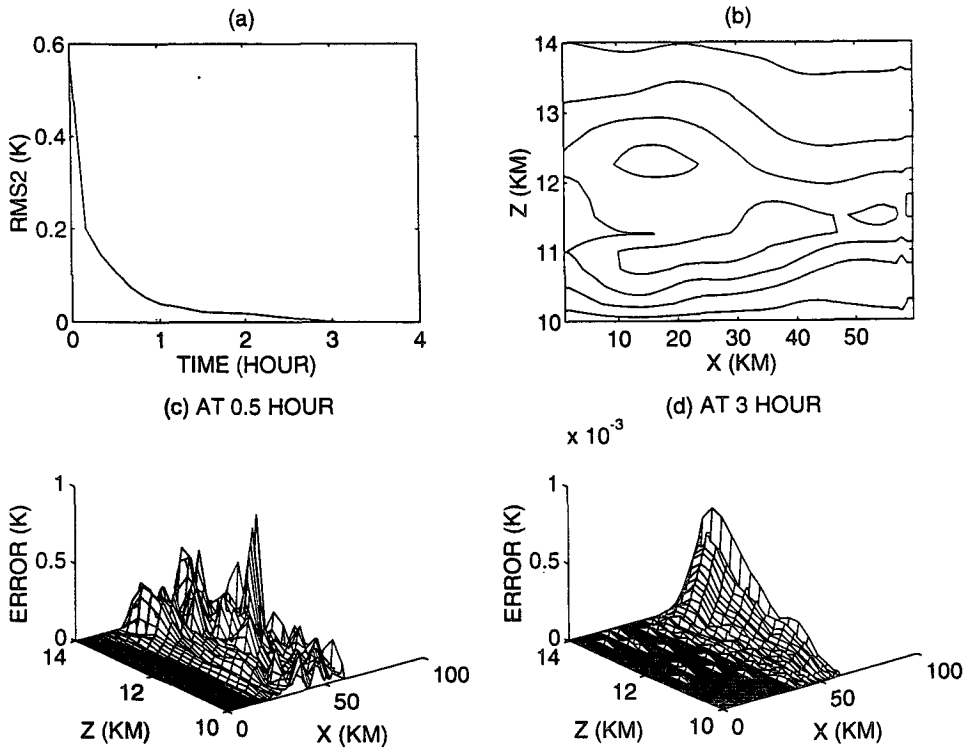

FIG. 8. (a) Error evolution of potential temperature field: prescribed lateral boundary conditions plus unidirectional flow. (b) Horizontal velocity pattern at 1 h showing unidirectional flow; maximum velocity is 28 m s^{-1}. (c) and (d) Error fields of potential temperature at 0.5 and 3 h.

tioned smaller-error strip, occupying the region of 60 km $\leqslant x \leqslant$ 120 km and 11 km $\leqslant z \leqslant$ 15 km, while the outer domain remains the same as before. We hoped to create inside the inner domain a flow pattern that is much more uniform, that is, unidirectional. In this case we expect to see much weaker error growth or even error decay. A relatively big random perturbation of [−1.0 K, +1.0 K] was introduced at every point and the model was run for 20 h. The rms2 for the potential temperature field is shown in Fig. 6a. Error decays to nearly zero at about 10 h and then grows, because the flow is quite uniform at the beginning, but during later hours there are larger return flows at the top, making the error grow (see horizontal velocity patterns in Figs. 7a–d). Figures 6b–d show the error fields of potential temperature at 5, 10, and 19 h, respectively (note the different vertical scales). It is obvious that error decays initially due to nearly unidirectional flow but grows later when more return flows appear at the top.

c. *Unidirectional flow pattern*

To make the error decay to zero, the return flow at the top of the inner domain must be removed. This is demonstrated in the following experiment in which the position of the inner domain is shifted 1 km downward to occupy the region of 60 km $\leqslant x \leqslant$ 120 km and 10 km $\leqslant z \leqslant$ 14 km. In this case there is no return flow in the domain, as shown in Fig. 8b. Again, a perturbation of [−1.0 K, +1.0 K] is introduced at every point. The rms2 for the potential temperature is shown in Fig. 8a. As expected, the error decays. The error fields at 0.5 and 3 h are plotted in Fig. 8c and 8d, which vividly show how the errors are removed from the domain. At t = 0.5 h, only about the left-hand quarter of the domain is free of error. At t = 3 h, the whole domain is virtually free of error except in the rightmost quarter. (Note, however, that the magnitude of the error is very small.)

4. Conclusions

Perturbation experiments have been performed using a numerical cloud model in equilibrium state, under both cyclic and prescribed lateral boundary conditions. It is shown that the model is very sensitive to initial conditions and some of the model parameters under cyclic boundary conditions. The fact that a very small perturbation (0.025°C) to the potential temperature at only one grid point can lead to rapid divergence of solutions (particularly in precipitation) suggests that the model is inherently sensitive to initial conditions. The model is also sensitive to model parameters such

as the cloud-to-rain conversion rate and the latent heat of vaporization. This study also addresses the question of why the initial perturbations can both grow and decay when prescribed lateral boundary conditions are imposed. It is shown that the prescribed lateral boundary conditions constrain error growth through the flow pattern in the domain. Errors decay when advected by unidirectional flow patterns resulting from the externally imposed lateral boundary conditions. Flow patterns with changing directions trap perturbations and lead to error growth. Neither domain size nor the prescription of lateral boundary conditions, taken alone, is sufficient to predict divergence or convergence of errors in the variables of the cloud model under study.

Acknowledgments. This research was supported by National Science Foundation under Grant ATM-9020832. Computational work was performed using supercomputing facilities at the National Center for Atmospheric Research, which is sponsored by NSF.

REFERENCES

Anthes, R. A., Y. H. Kuo, D. P. Baumhefner, R. M. Errico, and T. W. Bettge, 1985: Predictability of mesoscale motions. *Advances in Geophysics,* Vol. 28, Academic Press, 159–202.

Arakawa, A., 1966: Computational design for long term integration of the equation of motion: Two-dimensional incompressible flow. Part 1. *J. Comput. Phys.*, **1,** 119–143.

Berri, G. J., and J. Paegle, 1990: Sensitivity of local prediction to initial conditions. *J. Appl. Meteor.*, **29,** 256–267.

Charney, J. G., R. G. Feagle, H. Riehl, V. E. Lally, and D. Q. Wark, 1966: The feasibility of global observations and analysis experiment. *Bull. Amer. Meteor. Soc.*, **47,** 200–220.

Clark, T. L., 1977: A small scale dynamic model using a terrain-following coordinate transformation. *J. Comput. Phys.*, **24,** 186–215.

——, 1979: Numerical simulations with a three-dimensional cloud model: Lateral boundary condition experiments and multicellular severe storm simulations. *J. Atmos. Sci.*, **36,** 2191–2215.

——, and W. D. Hall, 1979: Numerical experiment on stochastic condensation theory. *J. Atmos. Sci.*, **36,** 470–483.

——, and W. R. Farley, 1984: Severe downslope windstorm calculations in two- and three-spatial dimensions using anelastic interactive grid nesting: A possible mechanism for gustiness. *J. Atmos. Sci.*, **41,** 329–350.

Errico, R., and D. Baumhefner, 1987: Predictability experiments using a high-resolution limited-area model. *Mon. Wea. Rev.*, **115,** 488–504.

Islam, S., 1991: Predictability of mesoscale precipitation. Sc.D. thesis, Department of Civil Engineering, Massachusetts Institute of Technology, Cambridge, 240 pp.

——, R. L. Bras, and K. A. Emanuel, 1993: Predictability of mesoscale rainfall in the Tropics. *J. Appl. Meteor.*, **32,** 297–310.

Jordan, C. L., 1958: Mean sounding for the West Indies area. *J. Meteor.*, **15,** 91–97.

Kasahara, A., 1972: Simulation experiments for the meteorological observing systems for GARP. *Bull. Amer. Meteor. Soc.*, **53,** 252–264.

Kessler, E., 1969: *On the Distribution and Continuity of Water Substance in Atmospheric Circulations. Meteor. Monogr.*, No. 32, Amer. Meteor. Soc., 84 pp.

Lilly, D. K., 1962: On the numerical simulation of buoyant convection. *Tellus,* **14,** 148–172.

——, 1965: On the computational stability of numerical solutions of time-dependent nonlinear geophysical fluid dynamics problems. *Mon. Wea. Rev.*, **93,** 11–26.

Paegle, J., and T. Vukicevic, 1987: On the predictability of low-level flow during ALPEX. *J. Meteor. Atmos. Phys.*, **36,** 45–60.

Smagorinsky, J., 1963: General circulation experiments with the primative equations. *Mon. Wea. Rev.*, **91,** 99–164.

Smolarkiewicz, P. K., 1984: A fully multidimensional positive definite advection transport algorithm with small implicit diffusion. *J. Comput. Phys.*, **54,** 325–362.

Tao, W.-K., and J. Simpson, 1989: A further study of cumulus interactions and mergers: Three-dimensional simulation with trajectory analysis. *J. Atmos. Sci.*, **46,** 2974–3004.

Vukicevic, T., and J. Paegle, 1989: The influence of one-way interacting lateral boundary conditions upon predictability of flow in bounded numerical models. *Mon. Wea. Rev.*, **117,** 340–350.

——, and R. M. Errico, 1990: The influence of artificial and physical factors upon predictability estimates using a complex limited-area model. *Mon. Wea. Rev.*, **118,** 1460–1482.

Zeng, X., and R. A. Pielke, 1993: Error-growth dynamics and predictability of surface thermally induced atmospheric flow. *J. Atmos. Sci.*, **50,** 2817–2844.